RESEARCH ARTICLE

Optimized Irreversibilities and Quartic Autocatalysis Chemical Reaction in A Wedge Flow

Sohail Rehman [1,*]

[1] Department of Physical and Numerical Sciences, Qurtuba University of Science and Information Technology, Peshawar, KP 25000, Pakistan

Abstract

Entropy optimization in the dissipative flow of a viscous liquid with a chemical species of quartic autocatalysis inside wedge geometry is investigated in this study by executing the revised Buongiorno model using numerical simulations. To demonstrate the feasibility of this approach, an illustration of the well-known model of laminar flow in the wedge domain of a planar surface is provided. The term for nanoparticles amalgamation in the heat equation is omitted, which accounts for additional involvement brought on by the migration of the nanoparticles in relation to the fluid. In addition, the energy released by autocatalysis processes is assumed to be insignificant. The studied nanofluid and chemical reactions are believed to be in a local thermal balance state. The dimensionless equations for flow, temperature, and concentration (nanoparticle volume fraction) are formulated and solved numerically using the Runge-Kutta (RK-4) approach. Findings suggest that fluid concentration is lowered with a rise in Schmidt number while temperature is enhanced with an elevation in heat source parameter. Thermal distribution and entropy rate are improved with a larger approximation of the radiation variable. The wedge parameter m depicts contrary effects for liquid velocity and concentration boundary layers while entropy depletion is seen.

Keywords: viscous material, wedge flow, heat and mass transfer, chemical reaction, entropy mechanism.

1 Introduction

Wedge flow is substantial in fluid dynamics and heat transport problems. The design of heat-transfer materials, drying systems, geothermal energy, nuclear systems, and many more systems are just a few examples of the variety of applications. Similar to the idealized layers of flocks and other types of porous materials that make up human lungs, biological systems having a wedge-like structure. In many industrial and medicinal purposes, wedge flows are crucial [1]. For instance, in the treatment of absent tissues and inadequate tumor volumes, wedge-shaped filters with isodoses transmission required in the anatomy of patients [2]. Initially, Falkneb and Skan [3] characterized the wedge-shape flow of a viscous and the associated boundary layers over a non-parallel plate. The dynamics of fluid with wall-bounded flows heavily relies on the Falkner and Skan model. It was

Submitted: 04 December 2025
Accepted: 18 February 2026
Published: 16 April 2026

Vol. 2, **No.** 2, 2026.
10.62762/JAM.2025.513035

***Corresponding author:**
✉ Sohail Rehman
srehman34@gatceh.edu; sohail@qurtuba.edu.pk

Citation
Rehman, S. (2026). Optimized Irreversibilities and Quartic Autocatalysis Chemical Reaction in A Wedge Flow. *ICCK Journal of Applied Mathematics*, 2(2), 137–152.

distinguished by the formation of a laminar boundary layer over a wedge when an exterior free stream velocity $V(x) \propto x$ exists, where the coordinate x extending beside the wedge geometry. They suggested a transformation method that results in a boundary value problem with the parameter $\gamma = 2m(m+1)^{-1}$, assessing the unfavorable or advantageous pressure differential. In order to explore the convection hydromagnetic flow around a wedge considering the consequences of heat sink/generation, Vajravelu and Nayfeh [4] enlarged the aforementioned problem. Yih [5] investigated forced convection, suction/blowing consequences, and non-isothermal wedge flow. In a heat walled wedge flow with forced convection, Chamkha et al. [6] investigated the effects of heat generating source and radiation heat. Ishak et al. [7] studied flow over a wedge with suction/blowing using the Falkner-Skan equation. Ibrahim and Tulu [8] provide numerical computation of the fluid layers flow over a wedge immersed in porous materials containing nanofluid with MHD and viscous dissipation effect used the spectrum quasilinearization techniques. The stretching wedge of the Casson fluid has recently been the subject of an analytical research by Bano et al. [9]. In a hybrid nanofluid with magnetohydrodynamics present, Waini et al. [10] investigated non-unique solutions on wedge shrinking and stretching. They discovered duality for the shrinking wedge scenario and established that the first solution is stable. A gigantic literature on the flows over a wedge can be viewed in [11–14].

The importance of optimizing heat transfer in industrial and engineering sectors has attracted a lot of attention in recent years. The majority of engineering machinery, including heat exchangers and electrical gadgets, traditionally uses heat transport fluids including ethylene glycol, water, and oil. Unfortunately, the reduced thermal conductance of these conventional fluids prevents the strengthening of heat transfer. Thermal scientists enhance the traditional fluids by adding various types of nanoparticles to develop a mixture referred as "nanofluid" which was first established by Choi [15], in order to overcome this problem. Studies have revealed that the nanomaterials have exceptional potential to improve the thermal conductivity and heat transfer rate of the base fluids. Since then, numerous scientists have investigated the heat transmission of a nanofluid for various features, either empirically or computationally. The behaviors of nanofluids have been predicted using a number of mathematical models, including the homogeneous flow models [15], the diffusion models [16], and the revised Buongiorno's model [17]. Since it illustrates the transportation mechanism among the base fluid and the nanoparticles quite effectively, Buongiorno's model gained the most attention among them. It is important to note that a number of researchers [14, 18, 19] have used homogeneous flow models to study boundary layer flows and heat transfer including autocatalysis reactions in nanofluids. Few studies have taken the Buongiorno's model of such nanofluid flow into consideration [20]. Only Zhao et al. [21] have elaborate the boundary layer flow of nanofluids close to a cylinder forward stagnation point in the presence of homogeneous-heterogeneous reaction in the literature. Only chemically reacting species B was taken into account in this study (heterogeneous reaction), while chemical species A was believed to be of normal size (homogeneous reaction).

Several chemical processes, including ignition, chemical synthesis, fuel cells, batteries, gas purification, and the formation of nanoparticles, involve both heterogeneous and homogeneous processes. With the use of a catalyst, the reaction is started. Homogeneous and heterogeneous processes interact very complicatedly on catalytic surfaces. These reactants involve different rates of synthesis and consumption both inside the liquid and on the catalytic surfaces. By taking viscous fluid, Chaudary and Merkin [22] created a straightforward isothermal model for the autocatalysis reaction in BLF. For a number of boundary layer flow problems over various geometrical structures, Xu et al. [23] mathematical modelis employed [18, 24, 25]. For a deeper understanding of homogeneous-heterogeneous reactions on nanofluids, readers are encouraged to consult Refs. [26–28].

Magnetohydrodynamic (MHD) for conduit flows have been an enduring focus of exploration over decades due to its significance in engineering solicitations such as electromagnetic molding, metallurgical solicitations, originators and the cooling blankets of magnetic captivity nuclear fusion reactors etc. [29, 30]. The coupling of the induced current with the magnetization creates in a Lorentz force, which acts on electrically conducting fluids flowing in the strong magnetic field. The turbulence fluctuations are dampened by this force, laminarizing the flow and reducing convicted heat transport in these ducts [31, 32]. Additionally, nanofluids exposed to magnetic fields have great potential for use in industries like geothermal energy extraction, nuclear reactor liquid-metal cooling, electromagnetic molding, flow meters, and generators as well as in fields like cancer treatment, asthma, and drug relief. Magnetic fields can prompt currents in moving conductive liquids, polarizing the fluid and altering the magnetic field in a reciprocal way. MHD is taken into account by investigators in their models since it is thought to be one of the key factors that would boost thermal conductivity in the fluid flow [33]. The coupling of the magnetic and velocity field results in the development of electrically conducting fluid by releasing forces operating on the fluid and reshaping the magnetic field while also causing the currents to flow in a nanofluid manner. Therefore, the tendency of MHD is completely described by the momentum and energy differential equations, which include the Navier-Stokes equations and Maxwell's equations. The involvement of a magnetic field relates with the velocity through the Lorentz force in the governing flow and temperature fields. Several scholars conducted investigations on MHD flow in the subsequent decades to determine the effects of the wedge flow by combining several other physical features [31, 34–36].

Radiant heat is the main contributor to thermal transfer. The functionality of radiation is remarkably focused on surface characteristics and solid geometry issues. Additionally, radiation plays a significant role in a number of engineering technologies, including waste heat storage, nuclear reactors, missile technology, furnace design, and missile technology, processes requiring high temperatures, oil shale sun pond distillation, combustion, and many others. Thermal radiation can also function as a heat-controlling agent in many industrial processes. Researchers have investigated numerous flow patterns to model these types of problems with distinct properties in light of the extensive use of radiations.

The ideal condition for a heat exchanger design is greater heat transfer coupled with less pressure loss. For any wedge, the gain in heat transmission is typically accompanied by a bigger increase in friction loss, which causes a higher rate of frictional entropy formation. In order to elaborate the optimal heat exchanger model, several researchers have tried to maximize heat transfer and thermodynamic enactment while decreasing friction loss and entropy production. The publications show that despite multiple efforts, the energy losses of cavitation, wedge flow, the flow field specifics of cavitation flow, and its generated dynamic attributes and wedge energy performance are not fully understood. In the past, a number of techniques to assess hydraulic losses in fluid machinery have been put forth in an effort to comprehend energy transmission. However, since the first rule of thermodynamics is the foundation of the conventional approach to evaluating the operation of fluid machinery, it is unable to account for the impact of irreversibility on hydraulic energy loss. Bejan and Kestin [37, 38] suggested a method for figuring out the entropy production rate produced by heat and fluid friction in a typical heat exchanger. The lowest entropy production was subsequently used as a gauge for the best thermal system structure, which has been discussed experimentally and theoretically by a number of researchers [39–41].

To the best of our knowledge, no study has investigated the mechanisms by which local entropy and irreversibility in systems with magnetohydrodynamic and quartic autocatalysis influence on the physical characteristics of nanofluids in a wedge flow topology. To explore the boundary-layer migration of nanofluids over a wedge surface when there is a mixture of homogeneous-heterogeneous reactions, Chaudhary and Merkin's autocatalysis reactant model and Buongiorno's nanofluid model were both incorporated. $\hat{A}$ and $\hat{B}$, two chemical species, are both nanoscale. This study used non-equilibrium thermodynamics in reaction-diffusion systems to perform entropy minimization topology, exergy loss of wedge flow distribution, and radiant heat. Fluid mechanic analyses may be supplemented with certain thermodynamic ideas with regard to the irreversible processes involved in order to better understand the physics of these loss-producing phenomena. These theories basically measure the value of energy in terms of how easily it can be converted between different forms. Entropy can be minimized but cannot be fully destructed because of the second law of thermodynamics. In a reversible process, exergy is therefore retained, but irreversibilities (such as losses in a flow or temperature field) result in exergy loss (in favor of the correspondingly increasing energy). With the assistance of these ideas, we intend to determine the entropy generation and, consequently, the losses in the flow through a wedge with smooth walls. Entropy optimization will be evaluated for the initial time in conjunction with the aforementioned model as we model utilizing the mass-based procedure. For some values of the controlling parameters, the Runge-Kutta-Fehlberg (RKF) method is combined with a standard shooting routine to numerically solve the modified normalized equations under the pertinent boundary conditions. The effect of controlling factors on the liquid flow and heat transfer characteristics of the problem are provided and analyzed in charts and graphical representations. The findings were found to be in good settlement with earlier development.

2 Overview and Formulation

The physical model structure for the assumed problem is depicted in Figure 1. An incompressible and electrically conductive fluid with electrical conductivity σ, kinematic and dynamic viscosity ν and μ flowing in a wedge. The main stream of the flow is parallel to the x-axis and y coordinate is located normal to the stream. The mainstream velocity and wall velocity are assumed to be $V_e(x) = V_\infty x^m$ and $V_w(x) = V_o x^m$, where V_∞ is the free stream velocity and m is positive constant $(1 \geq m \geq 0)$. The wedge angle is supposed to be $\beta = \pi\gamma$. In the outlook of White [42], positive values of γ specifies that the pressure differential is encouraging, while negative γ suggest that the flow will be accelerating towards the wedge apparent. Negative values of γ displays that the pressure differential is adversarial then the flow will be slow down. Furthermore, $\gamma = 0$, indicate the boundary layer flow over a flat horizontal surface, while $\gamma = 1$ correspond to stagnation point flow along a vertical surface. The free stream and wall temperature are assumed to be uniform and constant i.e., T_w and T_∞. The magnitude of magnetic field B is determined orthogonal to the wedge wall and in the y-positive axis direction. By supposing it to be extremely small in contrast to the applied magnetic field, the induced magnetic field is omitted. Additionally, $m = \frac{\gamma}{2-\gamma}$ where γ is the Hartree pressure gradient parameter that corresponds $\beta = \pi\gamma$. Based on aforementioned assumption the constituent equation for mass, momentum and energy conservation for boundary layer problem are given below. Surface charge agents (or surfactants) are used to assimilate the tiny nanoparticles into the base fluid in order to prevent agglomeration and deposit of the nanoparticles on the wedge media. In order to make the induced magnetic field and the Hall effects insignificant, it is supposed that the transverse applied magnetic field and magnetic Reynolds number are very tiny. High viscous flows or high velocity gradient flows require consideration of viscous dissipation. No slippage occurred among the fluid and the nanoparticles, which are in a condition of thermal equilibrium.

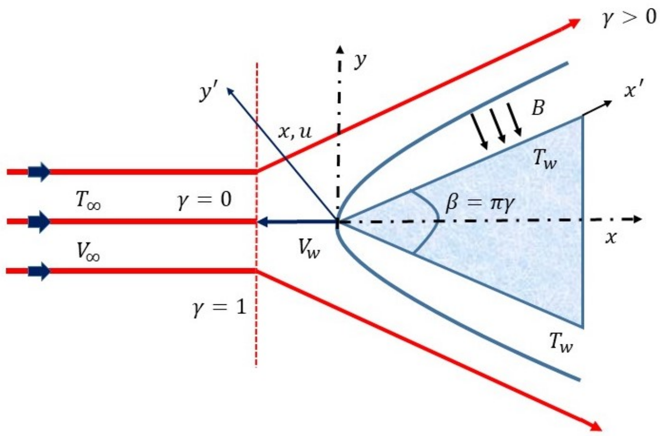

Figure 1. Schematic diagram of the physical model and coordinate system.

Following Chaudhary and Merkin assumption that the process is cubic isothermal autocatalytic in the bulk, which is denoted by:

$$\hat{A} + 2\hat{B} \rightarrow 3\hat{B}, \quad \text{rate} = K_1 a b^2, \tag{1}$$

whereas the isolated, first-order reaction on the catalyst surface is regulated by:

$$\hat{A} \rightarrow \hat{B}, \quad \text{rate} = K_s a, \tag{2}$$

Under those assumptions, the following constitutive relations can be used to describe the wedge flow of a nanofluid in the existence of autocatalytic reactions [14, 36]:

$$\nabla \cdot \vec{V} = 0, \tag{3}$$

$$\rho\left(\frac{DV}{Dt}\right) = -\nabla p + \nabla \cdot (\mu \nabla \vec{V}) + \vec{J} \times \vec{B}, \tag{4}$$

$$(\rho c_p)\left(\frac{DT}{Dt}\right) = \kappa \nabla^2 T + \Phi + \frac{\rho^2}{\sigma} + q'', \tag{5}$$

In above equations, p is the pressure, $\vec{V} = (u, v, 0)$ is the velocity field. The velocity components in the axial x and transverse y directions respectively.

$$\vec{V} = \frac{\partial}{\partial x}\hat{i} + \frac{\partial}{\partial y}\hat{j} + \frac{\partial}{\partial z}\hat{k},$$

is the del operator.

$$\frac{D}{Dt} = \frac{\partial}{\partial t} + (\vec{V} \cdot \nabla),$$

is the material derivative.

According to generalized Ohm's law [43]:

$$\vec{J} \times \vec{B} = \sigma\left[(\vec{E} + \vec{V} \times \vec{B}) - \frac{1}{e_m}\vec{J} \times \vec{B}\right], \tag{6}$$

where $\vec{J}$ denote the current density, $\vec{E}$ is the electric current density and it is assumed zero in the present model i.e., no voltage is applied, $\vec{B}=(0,0,B)$ is the magnetic field strength, e_m is the charge on an electron and n the number density of an electron,

$$\frac{Q_0(T-T_\infty)}{(\rho c_p)}$$

is the heat source/sink expression.

$$\vec{J}\times\vec{B}=-\frac{\sigma B^2 u}{\rho}, \tag{7}$$

Joule heating is illustrated by the expression

$$\frac{I^2}{\sigma}=\frac{IJ}{\sigma}=\frac{B^2u^2}{\sigma}, \tag{8}$$

The expression for Φ in the energy equation illustrate power per unit volume generated by viscous dissipation given by

$$\Phi=2\mu A_{ij}A_{ij}=\mu\frac{\partial^2 u}{\partial y^2}, \tag{9}$$

where $A_{ij}=\frac{1}{2}(V_{i,j}+V_{j,i})$, is the strain rate tensor.

Here, ρ, μ, κ, σ and (ρc_p) described the liquid density, dynamical viscosity, thermal conductivity, electrical conductivity and heat capacitance of the nanoLiquids [11, 36, 44].

$$\frac{\partial u}{\partial x}+\frac{\partial v}{\partial y}=0, \tag{10}$$

$$u\frac{\partial u}{\partial x}+v\frac{\partial v}{\partial y}=V_e(x)\frac{\partial V_e(x)}{\partial x}+\nu\frac{\partial^2 u}{\partial y^2}-\frac{\sigma_f B^2 u}{\rho}, \tag{11}$$

$$\begin{aligned} u\frac{\partial T}{\partial x}+v\frac{\partial T}{\partial y}&=\alpha\frac{\partial^2 T}{\partial y^2}+\frac{\mu}{(\rho c_p)}\left(\frac{\partial u}{\partial y}\right)^2\\ &-\frac{1}{(\rho c_p)}\frac{\partial q_r}{\partial y}+\frac{B^2u^2}{(\rho c_p)}+\frac{Q_0(T-T_\infty)}{(\rho c_p)}, \end{aligned} \tag{12}$$

$$u\frac{\partial a}{\partial x}+v\frac{\partial a}{\partial y}=D_A\frac{\partial^2 a}{\partial y^2}+\frac{D_T}{T_\infty}\frac{\partial^2 T}{\partial y^2}-K_1ab^2, \tag{13}$$

$$u\frac{\partial b}{\partial x}+v\frac{\partial b}{\partial y}=D_B\frac{\partial^2 b}{\partial y^2}+\frac{D_T}{T_\infty}\frac{\partial^2 T}{\partial y^2}+K_1ab^2, \tag{14}$$

The associated boundary conditions are:

$$\begin{aligned} &u=V_w(x)=V_o x^m,\quad v=0,\quad T=T_w,\\ &D_{\tilde{A}}\frac{\partial a}{\partial y}=-K_s a,\quad D_{\tilde{B}}\frac{\partial b}{\partial y}=K_s a\quad \text{as } y\to 0, \end{aligned} \tag{15}$$

$$\begin{aligned} &u=V_e(x)=V_\infty x^m,\quad T=T_\infty,\\ &a\to a_\infty,\quad b\to 0,\quad \text{as } y\to\infty, \end{aligned} \tag{16}$$

where K_1, K_s are coefficients related to the homogeneous, heterogeneous processes, respectively, and $\tilde{A}$ and $\tilde{B}$ are two distinct species of autocatalysts. It is anticipated that species $\tilde{B}$ does not happen in ambient liquid in order to meet the requirements of real-world circumstances. For ease of explanation, it is expected that the species $\tilde{A}$ far-field concentration a_∞ is constant. It is well known that all chemical reactions take place in the boundary layer and never in the distant field. Contrarily, Buongiorno discovered that the amount of heat transfer caused by nanoparticle dispersal pales in contrast to heat transportation and convection. We thus follow his recommendation and remove the factor referring to nanoparticle distribution from the energy equation in order to account for the additional contribution generated by the nanoparticles motion in respect to the fluid. We also ignore the portion of the energy equation that deals with heat transfer because we think that the energy produced by chemical reactions is negligible.

Using the Rosseland approach [45], the radiation intensity flow q_r is as follows:

$$q_r=-\frac{4\sigma^*}{3\kappa^*}\frac{\partial T^4}{\partial y}\approx-\frac{16\sigma^* T^4}{3\kappa^*}\frac{\partial T}{\partial y}, \tag{17}$$

With the aid of Eq. (17), the energy equation takes the form:

$$\begin{aligned} u\frac{\partial T}{\partial x}+v\frac{\partial T}{\partial y}&=\alpha\frac{\partial^2 T}{\partial y^2}+\left(\frac{\mu}{\rho c_p}\right)^2\left(\frac{\partial u}{\partial y}\right)^2\\ -\frac{1}{\rho c_p}\frac{\partial}{\partial y}\left(-\frac{16\sigma^* T^4}{3\kappa^*}\frac{\partial T}{\partial y}\right)&+\frac{B^2u^2}{\rho c_p}+\frac{Q_o(T-T_\infty)}{\rho c_p}, \end{aligned} \tag{18}$$

where T indicates the liquid temperature, ν is its kinematic viscosity, V_e is its velocity in the exterior flow, α is the thermal diffusivity, D_A and D_B are its thermal diffusion coefficient.

Incorporating the similarity variables:

$$\begin{aligned} &\zeta=y\sqrt{\frac{(m+1)V_e(x)}{2\nu x}},\quad u=V_e(x)f'(\zeta),\\ &\psi=\sqrt{\frac{2\nu x V_e(x)}{(m+1)}}f,\quad \Theta=\frac{T-T_\infty}{T_w-T_\infty},\\ &\Psi=\frac{a}{a_w},\quad \chi=\frac{b}{b_w}. \end{aligned} \tag{19}$$

Eqs. (11-14) and Eq. (18) are reduced into dimensionless form by invoking Eq. (19), thus we have

$$f'''+ff''+\frac{2m}{m+1}(1-f'^2)+\frac{2m}{m+1}M(1-f')=0, \quad (20)$$

$$\frac{1}{Pr}\left(1+\frac{4}{3}R_d\right)\Theta''+\frac{m+1}{2}\left(f\Theta'+Ec\,f'^2+M^2f'^2\right) + Q\Theta=0, \quad (21)$$

$$\Psi''+Sc\,\Psi' f-\frac{2m}{m+1}Sc\,\tilde{K}\,\Psi\chi^2=0, \quad (22)$$

$$\epsilon\chi''+Sc\,\chi' f+\frac{2m}{m+1}Sc\,\tilde{K}\,\Psi\chi^2=0, \quad (23)$$

$$\begin{aligned} &f(0)=1, \quad f'(0)=0, \quad \Theta(0)=0,\\ &\Psi'(0)=K_c\Psi, \quad \epsilon\chi'(0)=-K_c\Psi, \end{aligned} \quad (24)$$

$$f'(\infty)=1, \quad \Theta(\infty)=0, \quad \Psi(\infty)=1, \quad \chi(\infty)=0, \quad (25)$$

Here, M indicates the magnetic parameter, Q is the heat generating term, Pr elucidates the Prandtl number, m is the wedge angle, R_d is dimensionless radiative source, Ec is the Eckert number, Re represents the Reynolds number, Sc for Schmidt number, ϵ is the diffusion coefficients ratio, $\tilde{K}$ is the homogeneous reaction strength, K_c is the strength of heterogeneous reaction, respectively.

$$\begin{aligned} &M=\frac{2\sigma B^2x^{1-m}}{\rho v_\infty}, \; Q=\frac{2Q_0x}{(\rho c_p)(m+1)V_e}, \; Pr=\frac{\nu}{\alpha},\\ &m=\frac{\gamma}{2-\gamma}, \; R_d=\frac{4\sigma T_0^3}{\kappa^*\kappa}, \; Ec=\frac{V_e^2}{c_p\Delta T}, \; Re=\frac{V_ex}{\nu},\\ &Sc=\frac{\nu}{D_A}, \epsilon=\frac{D_{\tilde{A}}}{D_B}, \; \tilde{K}=\frac{K_1a_w^2x^2}{\nu}, \; K_c=\frac{K_sx^2}{D_{\tilde{A}}}. \end{aligned} \quad (26)$$

The diffusion coefficient terms are supposed to be identical i.e., $D_{\tilde{A}}=D_{\tilde{B}}$, so the ratio $\epsilon\to 1$.

Hence [46]

$$\Psi(\zeta)+\chi(\zeta)=1, \quad \text{or} \quad \chi(\zeta)=1-\Psi(\zeta). \quad (27)$$

Using Eq. (26) in Eqs. (22) and (23), we have

$$\Psi''+Sc\,\Psi' f-\frac{2m}{m+1}Sc\,\hat{K}\Psi(1-\Psi)^2=0, \quad (28)$$

$$\Psi'(0)=K_c\Psi(0), \quad \Psi(\infty)=1. \quad (29)$$

The practical interest quantities i.e., the skin drag force and heat transfer rate are:

$$\begin{aligned} &\sqrt{\frac{2Re}{m+1}}C_f=f''(0),\\ &\sqrt{\frac{2}{(m+1)Re}}Nu=-\left(1+\frac{4}{3}R_d\right)\Theta'(0), \end{aligned} \quad (30)$$

3 Entropy Production Optimization

Here, irreversible entropy production optimization for heterogeneous-homogeneous processes in nanofluid flow is carried out. On entropy production analysis, viscous dissipation effect is also induced. Dimensional configuration is impacted by these factors as reported in [47, 48].

$$\begin{aligned} S_G'''=&\frac{\kappa}{T_\infty^2}\left(1+\frac{16\sigma^*T^3}{3\kappa^*\kappa}\right)\left(\frac{\partial T}{\partial y}\right)^2+\frac{\mu}{T_\infty}\left(\frac{\partial u}{\partial y}\right)^2\\ &+\frac{\sigma B^2u^2}{T_\infty}+\frac{R_1D_A}{a}\left(\frac{\partial a}{\partial y}\right)^2+\frac{R_1D_B}{b}\left(\frac{\partial b}{\partial y}\right)^2\\ &+\frac{R_1D_A}{T_\infty}\left(\frac{\partial a}{\partial y}\right)\left(\frac{\partial T}{\partial y}\right)+\frac{R_1D_B}{T_\infty}\left(\frac{\partial b}{\partial y}\right), \end{aligned} \quad (31)$$

where the confined entropy production rate is defined as

$$N_G=\frac{S_G}{S_G'}=\frac{\kappa(T_w-T_\infty)^2}{x^2T_\infty^2}, \quad (32)$$

The dimensionless form of above entropy equation is settled as

$$\begin{aligned} N_G=&\left(\frac{m+1}{2}\right)Re\left[\left(1+\frac{4}{3}R_d\right)\Theta'^2+\frac{Br}{\delta}f''^2\right]\\ &+\frac{ReBrMf'^2}{\delta}\\ &+\left(\frac{m+1}{2}\right)\left[(\beta_a-\beta_b)\Theta'\Psi'+\frac{\Psi'^2}{\delta}\left(\frac{\beta_a}{\Psi}-\frac{\beta_b}{1-\Psi}\right)\right], \end{aligned} \quad (33)$$

$$\begin{aligned} &Br=\frac{\nu V_e^2}{\alpha c_p\Delta T}, \quad \beta_a=\frac{R_1D_Aa_w}{\kappa},\\ &\beta_b=\frac{R_1D_Ba_w}{\kappa}, \quad \delta=\frac{T_w-T_\infty}{T_\infty}, \end{aligned} \quad (34)$$

Table 1. Skin friction comparison with existing studies for diverse values of wedge angle m.

Reference	m					
	0	0.09	0.2	0.3	0.5	1
Watanabe [52]	0.46960	0.65498	0.80213	0.92765	-	-
Yih [5]	0.469600	0.654979	0.802125	0.927653	-	1.232588
Yacob et al. [53]	0.469599	0.654994	0.802126	0.927680	1.038903	1.232588
Berrehal et al. [54, 55]	0.469599	0.654993	0.802125	0.927680	1.038903	1.232587
Berrehal et al. [11]	0.469599	0.654994	0.802126	0.927680	1.038903	1.232588
Present results	0.469501	0.654916	0.802120	0.927639	1.038900	1.232523

4 Numerical Scheme and Justification

A boundary value problem (BVP) is more challenging to solve than an initial value problem (IVP) [49]. The fourth order Runge-Kutta (RK-4) method is typically used to solve BVP numerically after it has been transformed to an IVP [49]. The governing equations (20), (21) and (27) have a nonlinear structure. In order to tackle these equations numerically under the boundary conditions (24) and (25) we must use the RK-4 technique along with the shooting method. The appropriate hypothetical values for border situations are picked in order to integrate (24) and (25) as an IVP.

To roughly compute the missing opening inclination at the boundary, shooting technique is used. By using the fourth order RK-4 process with grid size $h = 0.01$ and correcting the measured values, a better judgement of the answer is produced (uniform grid has been used). To satisfy the convergence conditions of 10^{-6}, the aforementioned act is reviewed. In order to satisfy the boundary criteria asymptotically, the asymptotic far field border conditions given by Eqs. (25) and (28) at $\zeta \to \infty$ were selected. Iterations are carried out with $\zeta_\infty = 5$ instead of $\zeta \to \infty$ with a convergence threshold of 10^{-6} being used in all circumstances. For all organized consequences, it delivers approximately four decimal places of accuracy. One can find detailed reports on the method in [50, 51]. Comparing the shooting approach to others, it produces proper results for precise guess values.

To authenticate the present computational scheme, Tables 1 and 2 present the normalized skin friction $f''(0)$ and heat transfer rate Nu in limiting situation (static wedge), when $R_d = 0$. Tabulated results show an excellent agreement with existing literature.

Table 2. Heat transfer rate comparison with existing studies for diverse values of wedge angle m.

Reference	m	
	0	1
Kuo [56]	0.8673	1.1147
Butt et al. [57]	0.8673	-
Khan et al. [58]	0.8769	1.1279
Berrehal et al. [54, 55]	0.876898	1.127959
Berrehal et al. [11]	0.876909	1.127964
Present results	0.876921	1.129021

5 Results and Discussion

Here, we used the Newton built-in-Shooting technique to generate nonlinear systems using the numerical results. This section looks at the characteristics of variables that have an impact on velocity, temperature, entropy generation rate, and concentration. Intriguing variables are used to assess numerical findings for surface drag force and temperature gradient.

The impact of the magnetic number (M) on the velocity mechanisms is illustrated in Figure 2. The major velocity constituent decreases as the magnetic number rises, but the velocity itself increases at the same time. This rise in velocity occurs as a result of the Hall current influence on the entire fluid region. As anticipated, when the magnetic number M is amplified, a decrease in the resulting velocity can be noticed. This is due to the conventional conclusion, according to which the magnetic field appears to provide the Lorentz force immediately before the electrically conducting fluid moves up to the opposing force category. Maintaining these characteristics, the movements of the fluid stream in thicknesses ultimately reached a point where they slowed down. Physically, the Lorentz force develops stronger, which causes the intensity of the velocities to decrease. A repulsive force created by magnetic lines moving in

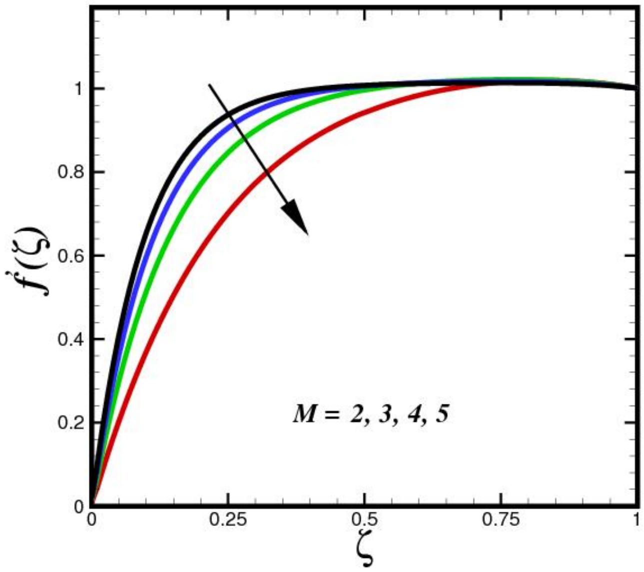

Figure 2. Trend of velocity $f'(\zeta)$ with different M.

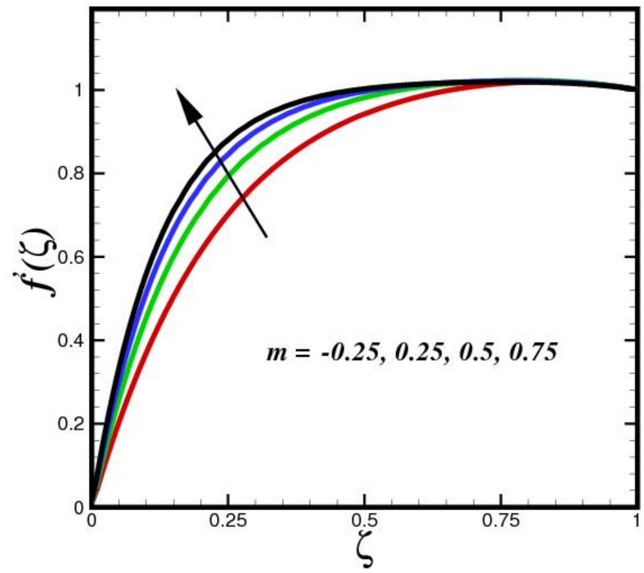

Figure 3. Trend of velocity $f'(\zeta)$ with different m.

relation to the wedge surface slow down the fluid motion. The profile of velocity for different values of wedge parameter m is displayed in Figure 3. It can be seen that the linear horizontal velocity is lowest for $m < 0$ and highest for $m > 0$. This is due to the fact that the elevation in the pressure gradient strengthens the expansion of the boundary layer and the formation of momentum on the wall. Hence, compared to flat plate flow, wedge flow $(m > 1)$ provides strong flow acceleration, although maximal flow acceleration is only possible with $(m = 1)$. At all values of m, the trend in velocity profiles is maintained. The thickness of the momentum boundary layer tends to decrease as the value of m increases. The fact that high values of m produce parabolic profiles is also noteworthy. Nevertheless, the acceleration is attained and maintained into the free stream with increasing distance from the wall. As a result, micro-rotation is highly sensitive to the pressure gradient parameter. The flat plate case that is closer to the wall and the forward stagnation flow case that is farther from the wall have the same maximum velocity.

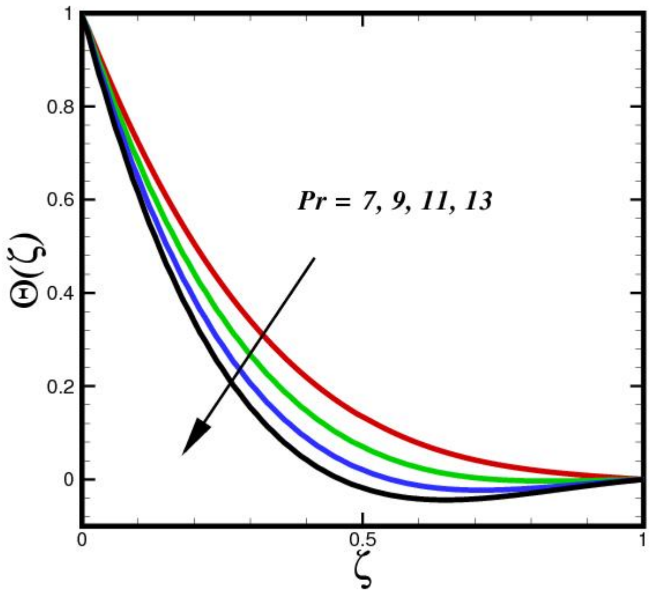

Figure 4. Trend of thermal field $\Theta(\zeta)$ with different Pr.

The temperature profile appears to decrease as the Prandtl number rises when glancing at the immediate temperature maps plotted in Figure 4. The importance of heat diffusion increases relative to eddy transport, particularly in the region close to the wall. The dampening of temperature variations and the dissipation of small scales are caused by the incremental diffusivity. As evidenced by the fact that the temperature map does not resemble the wedge flow structures at small scales, temperature patterns are fully attenuated at enhanced Pr. Due to the significant thermal diffusivity of the flow at low Prandtl numbers, as was discussed by Grötzbach [59], turbulent thermal diffusivity only surpasses molecular thermal diffusivity at an elevated Reynolds numbers $Re = 100$.

Figure 5 shows the temperature distributions for various values of m. The temperature is raised at all positions, from the wedge surface to the free stream,

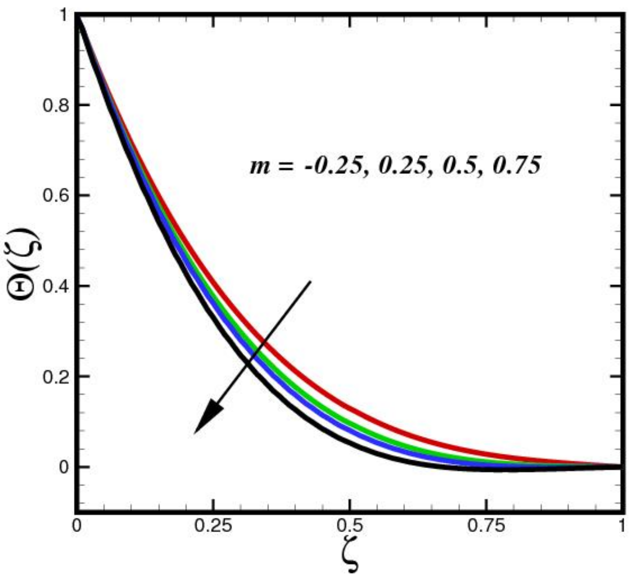

Figure 5. Trend of thermal field $\Theta(\zeta)$ with different m.

as a result of the improvement in m. Higher m causes profiles to become more parabolic in character. Temperature is minimized for vanishing pressure gradient (flat plate scenario, $m = 0$). The strongest pressure gradient, for which $m = 1$, results in its maximization. These other two examples are intercalated between the wedge case $(0 < m < 1)$. Hence, the thickness of the thermal boundary layer is maximal in the forward stagnation flow case and minimal in the flat plate (Blasius) case.

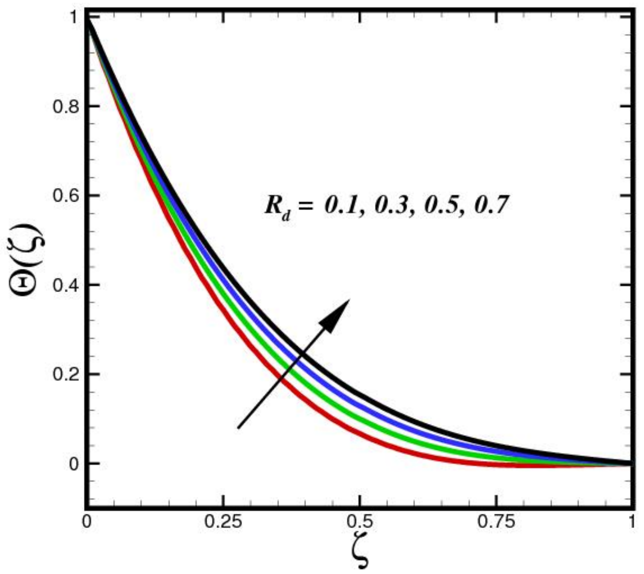

Figure 6. Trend of thermal field $\Theta(\zeta)$ with different R_d.

The temperature profile improves as the radiation parameter R_d increases, according to Figure 6. The nanofluids temperature rises because of the fluid increased heat emission as the radiation parameter value rises. The impact on boundary layer thickness, however, is nearly invisible, according to the study findings. To see the distinction, enlargement has been done. The thermal boundary layer's thickness increases in tandem with the rise in the radiation parameter.

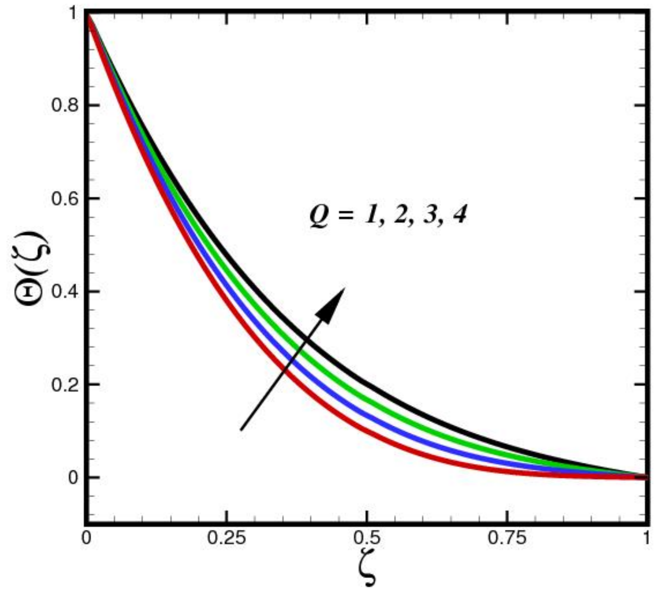

Figure 7. Trend of thermal field $\Theta(\zeta)$ with different Q.

Figure 7 illustrates how Q (source/sink) affects temperature. When a hot spot or cooled spot exists on the material being deposited to enable thermal energy management, this is a crucial effect in the treatment of nanomaterials. Heat generation by $Q > 0$ (increased thermal diffusion) causes the temperature to increase over time. Between $Q = 0$, $Q < 0$ and $Q > 0$ are the contours for Θ lies. According to these features, the boundary layer thickness increases during the "heat influence" on layers and decreases during the "cold effect" (cool effects). It is also interesting that, although all profiles once more converge smoothly in the free stream at the maximum value of the transverse coordinate, stronger temperature gradients are seen at higher positive values of this parameter.

The thermal profile line stream shows a positive trend when the Eckert number increases, as shown in Figure 8. Since the Eckert number indicates the ratio of kinetic energy comparable to the boundary layer enthalpy variation, more kinetic energy escapes in the

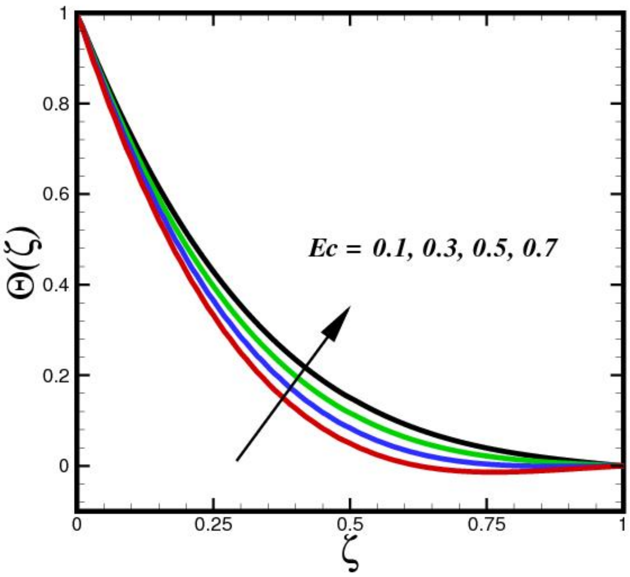

Figure 8. Trend of thermal field $\Theta(\zeta)$ with different Ec.

flow motion, which causes frictional heating.

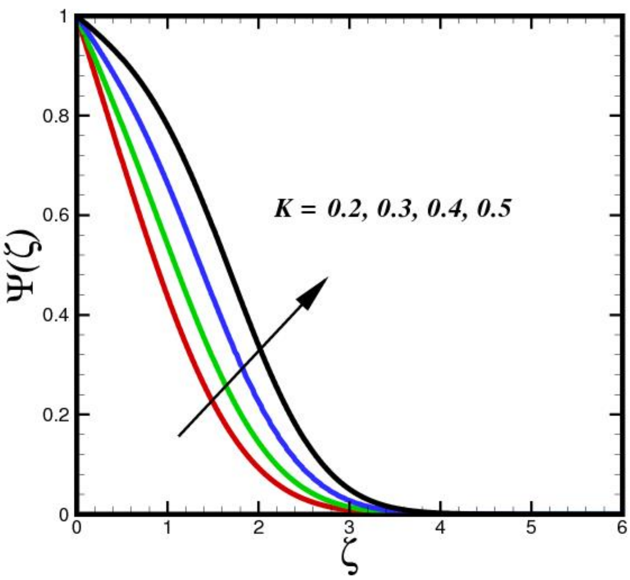

Figure 9. Trend of mass species $\Psi(\zeta)$ with different K.

In Figure 9, the influence K on $\Psi(\zeta)$ is depicted for the wedge flow case. The concentration profile was raised by the rise in K value. In this scenario, an increase in K is beneficial for boosting the chemical species concentration. The concentration of chemical species rises as the rate of change in velocity of a heterogeneous reaction does, indicating that more species that are chemical are participating in the process. Moreover, the reduction in fluid flow under the aggregation condition is slower for increasing values of K. Here, we find that fluid flow has higher mass transfer when an aggregation condition is present. It is observed that the concentration boundary layer expands greatly close to the wall before progressively contracting to meet the boundary requirement in the distant region. For higher levels of the K parameter, the increased chemical reaction in the boundary layer region enhances the concentration is shown.

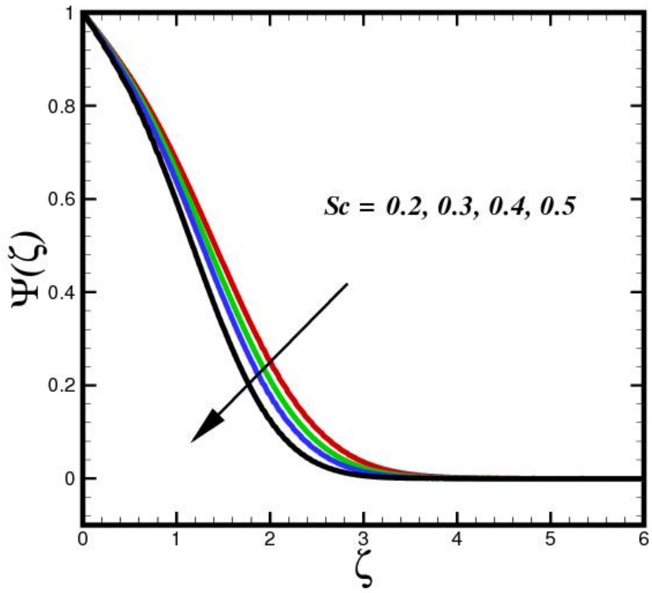

Figure 10. Trend of mass species $\Psi(\zeta)$ with different Sc.

The impact of Sc on $\Psi(\zeta)$ for a wedge flow is seen in Figure 10. The concentration profile diminishes as Sc value rises. The smallest Sc indicates the maximum nanoparticle concentration. As Sc escalations begin to initiate mass transfer to decrease, momentum diffusivity rises. Moreover, NPs aggregated fluid flow exhibits enhanced mass transfer compared to other fluid flows. Here, we find that fluid movement without NP aggregation results in the least amount of mass transfer.

The effect of the wedge angle parameter m on the concentration field $\Psi(\zeta)$ is depicted in Figure 11. The concentration profile increases slightly in direct relation to wedge wall proximity. An inclined arrow that shows a rising quantity of entity concentration for both static and changing border conditions can be seen. However, the influence of m on the concentration boundary layer is not sufficiently significant compared to its impact on velocity and temperature fields.

Figure 12 depicts the impact of entropy rate versus

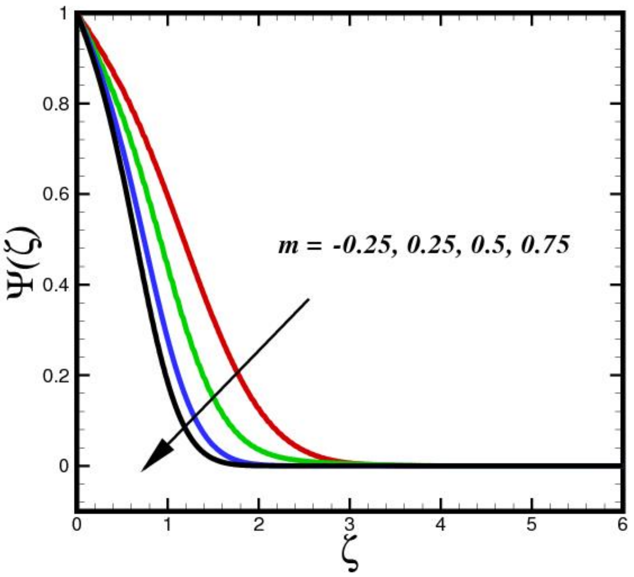

Figure 11. Trend of mass species $\Psi(\zeta)$ with different m.

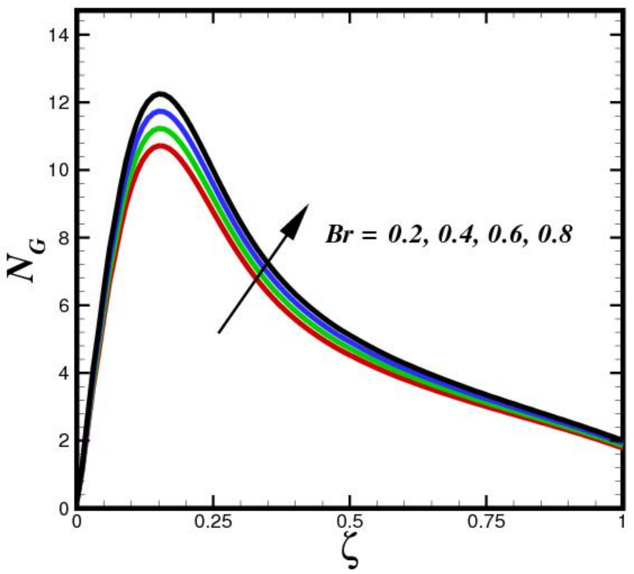

Figure 12. Trend of entropy rate $N_G(\zeta)$ with different Br.

(Br). An elevation in frictional forces as a result of a higher estimation of (Br) results in the production of more energy in the system, which increases the rate of entropy. Due to the fact that Prandtl and Eckert number are merged to produce the Brinkman number. As the Eckert number Ec increases, our findings show that entropy creation also increases. The irreversibility ultimately grows because of the increased kinetic energy that causes it to occur. In addition, based on the observation that the entropy generation rate increases as Prandtl number increases.

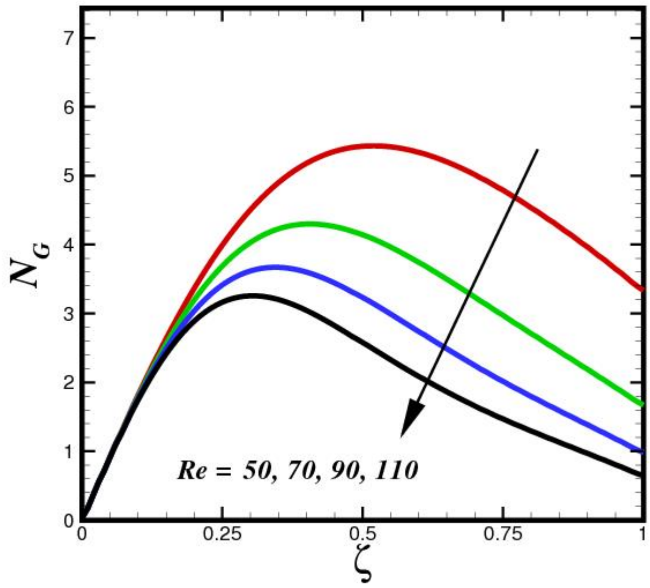

Figure 13. Trend of entropy rate $N_G(\zeta)$ with different Re.

In Figure 13, entropy generation is thoroughly examined for various Reynolds numbers and volume fractions of nano-additives. Temperature gradient and convective heat transfer are indirectly related in the constant heat flux boundary condition. Convective heat transfer rises by raising Reynolds numbers, as was previously described. Consequently, raising this value causes the temperature gradient to decrease. The creation of thermal entropy, on the other hand, is indirectly related to the temperature gradient. Consequently, it can be deduced that an increase in all study parameters can result in a decrease in the creation of thermal entropy. The pressure loss pattern is precisely followed by frictional entropy generation. Changes in the quantity of frictional entropy generation could be justified by taking into account the impact of rising Reynolds number on the evolution of the hydrodynamic boundary condition and velocity gradient. The aggregate of frictional and heat entropy generation results in the generation of total entropy.

The effect of entropy rate versus a magnetic field is highlighted in Figure 14. Higher magnetic effect approximations tend to augment drag force, which raises system energy. As a result, the entropy rate $N_G(\zeta)$ rises. The system-increased enthalpy, which eventually increases the irreversibility, causes it to occur.

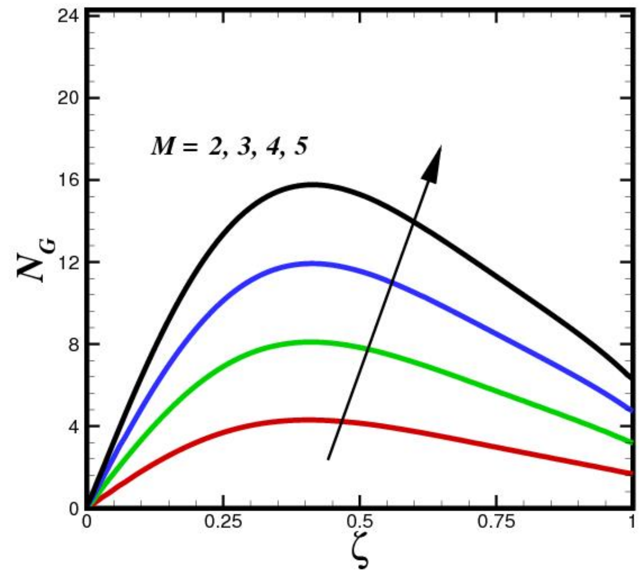

Figure 14. Trend of entropy rate $N_G(\zeta)$ with different M.

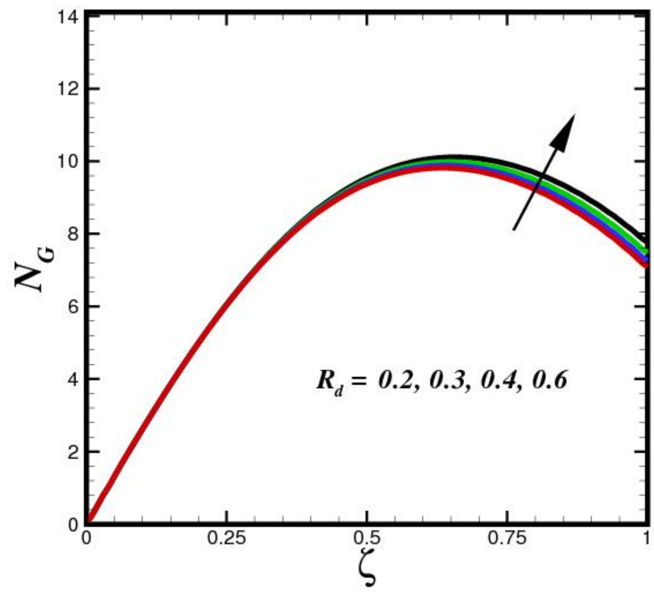

Figure 16. Trend of entropy rate $N_G(\zeta)$ with different Rd.

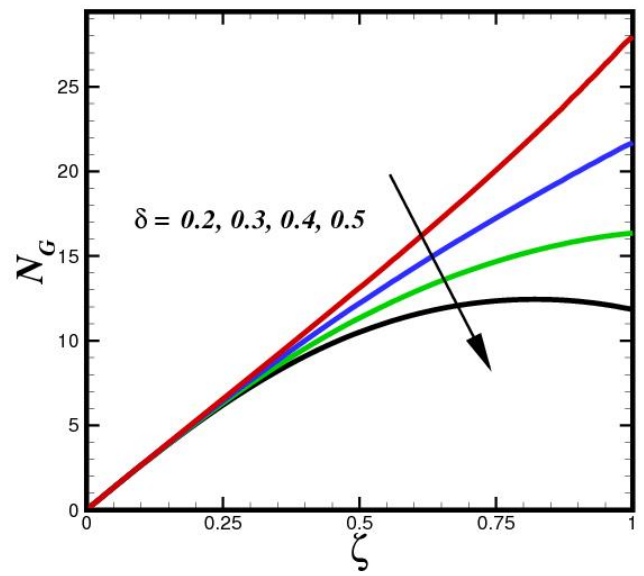

Figure 15. Trend of entropy rate $N_G(\zeta)$ with different δ.

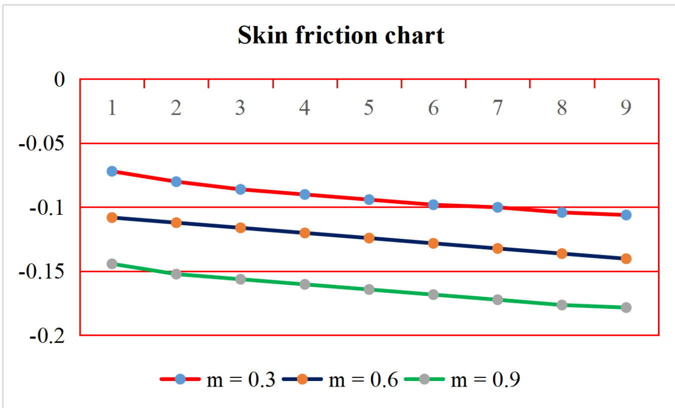

Figure 17. Evaluation of skin friction with various values of wedge parameter m.

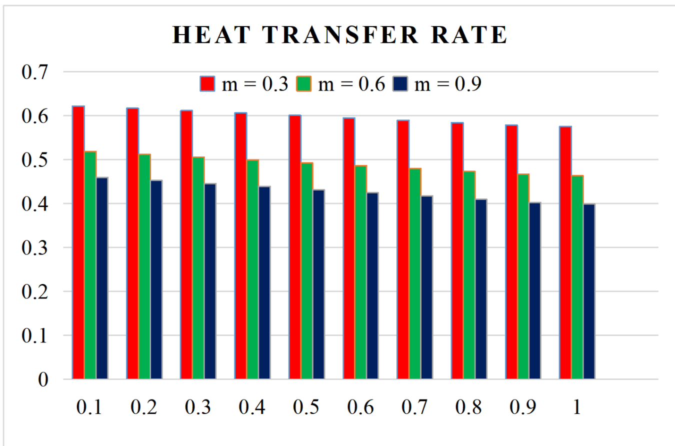

Figure 18. Evaluation of heat transfer rate with various values of wedge parameter m.

For the temperature difference ratio parameter δ, Figure 15 shows the entropy generation $N_G(\zeta)$ behavior. Entropy generation $N_G(\zeta)$ reduces when the temperature difference ratio parameter increases.

Figure 16 reports the effects of radiation on the entropy rate. Here, the radiation effect leads to an increase in entropy rate. The emission of radiation is amplified by a greater radiation (R_d) variable, which tends to intensify the collision between nanoparticles. Entropy rate increases as a result.

The wedge flow variable m influences the drag force inversely. Greater wedge angles that result in separation and less surface drag are indicated by higher values of m (Figure 17). Hence, m must be kept substantially larger in order to lessen the drag force on the wedge surface. Similar trend for heat transfer rate against wedge flow parameter (Figure 18). Heat transfer rate dwindles with enhancement of wedge parameter.

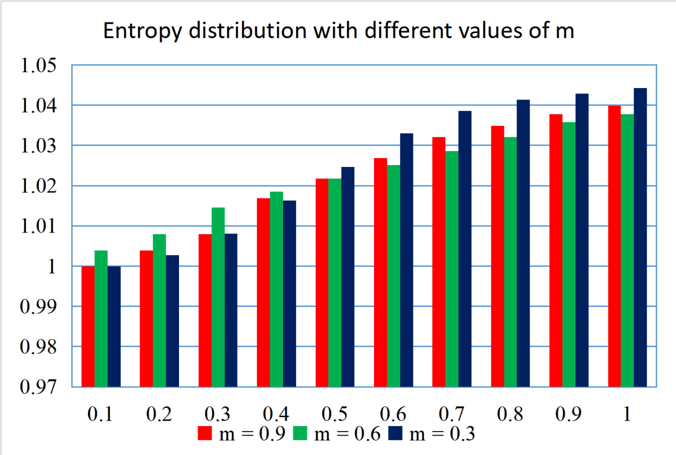

Figure 19. Evaluation of entropy distribution rate with various values of wedge parameter m.

We observed that the entropy generation has its lowest values at larger values of m, which corresponds to weak convection at borders (Figure 19). Thereafter, they start to increase until stability is attained at $m \to 1$. Evidently, the horizontal plate, wedge, and vertical plate are the three geometries that exhibit the same trend. As a result, lowering the wedge angle through boundaries can minimize entropy creation. In addition, the irreversibility of heat transfer takes over as the dominant property for the smallest m once the irreversibility of friction starts to back down with an increase in the wedge parameter.

6 Conclusion

The Buongiorno model approach integrated with R-K methodology is used to examine the mathematical model of entropy generation optimization in dissipative flow of nanofluid between wedge surface under the impact of Lorentz forces and chemical reaction of autocatalysis. The system of PDEs used to depict the mathematical flow model is then transformed into equivalent ODEs with the aid of similarity variables. The presented model approximate solution is computed in MATLAB program using the EG reference dataset, which is produced by altering various parameters. Additionally, it is supported by numerical and pictorial evidence. Velocity decreases with higher values of the magnetic parameter and increases with the wedge parameter. Increasing the estimates of the thermal radiation parameter improves the thermal field. By using higher magnetic parameter and Brinkman number values, entropy creation increases. In the wedge flow mechanisms, the distributions of dimensionless heat transfer and viscous friction entropy formation are fundamentally different. In addition, under the mutual impact of temperature and velocity field, the entropy generation under two mechanisms exhibits a symmetry property and periodic fluctuation, but the trends are in opposition to other geometries such as convergent channel. With its impact on the thermal and momentum mixing, the secondary flow makes a significant contribution to the formation of entropy. Higher estimation of wedge flow parameter significantly influence the skin friction rate, heat transfer rate and entropy production rate in a inverse manner.

Data Availability Statement

Data will be made available on request.

Funding

This work was supported without any funding.

Conflicts of Interest

The author declares no conflicts of interest.

AI Use Statement

The author declares that no generative AI was used in the preparation of this manuscript.

Ethical Approval and Consent to Participate

Not applicable.

References

[1] Nagendramma, V., Sreelakshmi, K., & Sarojamma, G. (2015). MHD heat and mass transfer flow over a stretching wedge with convective boundary condition and thermophoresis. *Procedia Engineering, 127*, 963–969. [CrossRef]

[2] Zhu, J. (2005). Generation of wedge-shaped dose distributions through dynamic multileaf collimator dose delivery. *Journal of Applied Clinical Medical Physics, 6*(3), 37–45. [CrossRef]

[3] Falkneb, V. M., & Skan, S. W. (1931). LXXXV. Solutions of the boundary-layer equations. *The London, Edinburgh, and Dublin Philosophical Magazine and Journal of Science, 12*(80), 865-896. [CrossRef]

[4] Vajravelu, K., & Nayfeh, J. (1992). Hydromagnetic convection at a cone and a wedge. *International Communications in Heat and Mass Transfer, 19*(5), 701–710. [CrossRef]

[5] Yih, K. A. (1998). Uniform suction/blowing effect on forced convection about a wedge: Uniform heat flux. *Acta Mechanica, 128*(3), 173–181. [CrossRef]

[6] Chamkha, A. J., Mujtaba, M., Quadri, A., & Issa, C. (2003). Thermal radiation effects on MHD forced convection flow adjacent to a non-isothermal wedge in the presence of a heat source or sink. *Heat and Mass Transfer, 39*(4), 305–312. [CrossRef]

[7] Ishak, A., Nazar, R., & Pop, I. (2007). Falkner-Skan equation for flow past a moving wedge with suction or injection. *Journal of Applied Mathematics and Computing, 25*(1), 67-83. [CrossRef]

[8] Ibrahim, W., & Tulu, A. (2019). Magnetohydrodynamic (MHD) boundary layer flow past a wedge with heat transfer and viscous effects of nanofluid embedded in porous media. *Mathematical Problems in Engineering, 2019*(1), 4507852. [CrossRef]

[9] Bano, N., Singh, B. B., & Sayyed, S. R. (2020). MHD heat transfer flow of Casson fluid with velocity and thermal slips over a stretching wedge in the presence of thermal radiation. *Diffusion Foundations, 26*, 1–22. [CrossRef]

[10] Waini, I., Ishak, A., & Pop, I. (2020). Transpiration effects on hybrid nanofluid flow and heat transfer over a stretching/shrinking sheet with uniform shear flow. *Alexandria Engineering Journal, 59*(1), 91–99. [CrossRef]

[11] Berrehal, H., Dinarvand, S., & Khan, I. (2022). Mass-based hybrid nanofluid model for entropy generation analysis of flow upon a convectively-warmed moving wedge. *Chinese Journal of Physics, 77*, 2603–2616. [CrossRef]

[12] Hussain, D., Asghar, Z., Zeeshan, A., & Alsulami, H. (2022). Analysis of sensitivity of thermal conductivity and variable viscosity on wall heat flux in flow of viscous fluid over a porous wedge. *International Communications in Heat and Mass Transfer, 135*, 106104. [CrossRef]

[13] Khan, W. A., & Pop, I. (2013). Boundary layer flow past a wedge moving in a nanofluid. *Mathematical Problems in Engineering, 2013*(1), 637285. [CrossRef]

[14] Rana, P., Gupta, S., & Gupta, G. (2023). FEM computations and Taguchi optimization in nonlinear radiative MHD MWCNT-MgO/EG hybrid nanoliquid flow and heat transfer over a 3D wedge surface. *Case Studies in Thermal Engineering, 41*, 102639. [CrossRef]

[15] Choi, S. U. (1995, November). Enhancing thermal conductivity of fluids with nanoparticles. In *ASME international mechanical engineering congress and exposition* (Vol. 17421, pp. 99-105). American Society of Mechanical Engineers. [CrossRef]

[16] Xuan, Y., & Roetzel, W. (2000). Conceptions for heat transfer correlation of nanofluids. *International Journal of Heat and Mass Transfer, 43*(19), 3701–3707. [CrossRef]

[17] Buongiorno, J. (2005). Convective transport in nanofluids. *Journal of Heat Transfer, 128*(3), 240–250. [CrossRef]

[18] Kameswaran, P. K., Shaw, S., Sibanda, P. V. S. N., & Murthy, P. V. S. N. (2013). Homogeneous–heterogeneous reactions in a nanofluid flow due to a porous stretching sheet. *International journal of heat and mass transfer, 57*(2), 465-472. [CrossRef]

[19] Hayat, T., Hussain, Z., Muhammad, T., & Alsaedi, A. (2016). Effects of homogeneous and heterogeneous reactions in flow of nanofluids over a nonlinear stretching surface with variable surface thickness. *Journal of Molecular Liquids, 221*, 1121-1127. [CrossRef]

[20] Zhang, C., Zheng, L., Zhang, X., & Chen, G. (2015). MHD flow and radiation heat transfer of nanofluids in porous media with variable surface heat flux and chemical reaction. *Applied Mathematical Modelling, 39*(1), 165–181. [CrossRef]

[21] Zhao, Q., Xu, H., & Tao, L. (2016). Homogeneous-heterogeneous reactions in boundary-layer flow of a nanofluid near the forward stagnation point of a cylinder. *Journal of Heat Transfer, 139*(3). [CrossRef]

[22] Chaudhary, M. A., & Merkin, J. H. (1995). A simple isothermal model for homogeneous-heterogeneous reactions in boundary-layer flow. I Equal diffusivities. *Fluid Dynamics Research, 16*(6), 311–333. [CrossRef]

[23] Xu, N. L., Xu, H., & Raees, A. (2018). Homogeneous-heterogeneous reactions in flow of nanofluids near the stagnation region of a plane surface: The Buongiorno's model. *International Journal of Heat and Mass Transfer, 125*, 604-609. [CrossRef]

[24] Raizah, Z. A. S., Ahmed, S. E., & Aly, A. M. (2020). ISPH simulations of natural convection flow in E-enclosure filled with a nanofluid including homogeneous/heterogeneous porous media and solid particles. *International Journal of Heat and Mass Transfer, 160*, 120153. [CrossRef]

[25] Hayat, T., Rashid, M., Imtiaz, M., & Alsaedi, A. (2017). Nanofluid flow due to rotating disk with variable thickness and homogeneous-heterogeneous reactions. *International Journal of Heat and Mass Transfer, 113*, 96–105. [CrossRef]

[26] Sravanthi, C. S., Mabood, F., Nabi, S. G., & Shehzad, S. A. (2022). Heterogeneous and homogeneous reactive flow of magnetite-water nanofluid over a magnetized moving plate. *Propulsion and Power Research, 11*(2), 265–275. [CrossRef]

[27] Waqas, H., Khan, S. U., Khan, M. I., Alzahrani, F., & Qayyum, S. (2021). Study of homogeneous–heterogeneous reactions in bioconvection stagnation point slip flow of Walter's-B nanofluid with nonlinear thermal radiation and activation energy. *International Communications in Heat and Mass Transfer, 129*, 105729. [CrossRef]

[28] Kumar, R., Kumar, R., Shehzad, S. A., & Sheikholeslami, M. (2018). Rotating frame analysis of radiating and reacting ferro-nanofluid considering Joule heating and viscous dissipation. *International Journal of Heat and Mass Transfer, 120*, 540–551. [CrossRef]

[29] Barleon, L., Casal, V., & Lenhart, L. (1991). MHD flow in liquid-metal-cooled blankets. *Fusion Engineering and Design, 14*(3-4), 401-412. [CrossRef]

[30] Müller, U., & Bühler, L. (2001). *Magnetofluiddynamics in channels and containers*. Springer Science & Business Media. [CrossRef]

[31] Murali, S., Hussam, W. K., & Sheard, G. J. (2021). Heat transfer enhancement in quasi-two-dimensional magnetohydrodynamic duct flows using repeated flow-facing wedge-shaped protrusions. *International Journal of Heat and Mass Transfer, 171*, 121066. [CrossRef]

[32] Waini, I., Ishak, A., & Pop, I. (2020). Flow and heat transfer of a hybrid nanofluid past a permeable moving surface. *Chinese Journal of Physics, 66*, 606-619. [CrossRef]

[33] Astanina, M. S., Sheremet, M. A., Oztop, H. F., & Abu-Hamdeh, N. (2018). MHD natural convection and entropy generation of ferrofluid in an open trapezoidal cavity partially filled with a porous medium. *International Journal of Mechanical Sciences, 136*, 493–502. [CrossRef]

[34] Raju, C. S. K., & Sandeep, N. (2016). Nonlinear radiative magnetohydrodynamic Falkner-Skan flow of Casson fluid over a wedge. *Alexandria Engineering Journal, 55*(3), 2045–2054. [CrossRef]

[35] Anantha Kumar, K., Ramana Reddy, J. V., Sugunamma, V., & Sandeep, N. (2018). Magnetohydrodynamic Cattaneo-Christov flow past a cone and a wedge with variable heat source/sink. *Alexandria Engineering Journal, 57*(1), 435–443. [CrossRef]

[36] Ali, L., Ali, B., Liu, X., Iqbal, T., Zulqarnain, R. M., & Javid, M. (2022). A comparative study of unsteady MHD Falkner–Skan wedge flow for non-Newtonian nanofluids considering thermal radiation and activation energy. *Chinese Journal of Physics, 77*, 1625–1638. [CrossRef]

[37] Bejan, A. (1996). Entropy generation minimization: The new thermodynamics of finite-size devices and finite-time processes. *Journal of Applied Physics, 79*(3), 1191–1218. [CrossRef]

[38] Bejan, A., & Kestin, J. (1983). Entropy generation through heat and fluid flow. *Journal of Applied Mechanics, 50*(2), 475. [CrossRef]

[39] Zhao, T., Hua, Y. C., & Guo, Z. Y. (2022). Irreversibility evaluation for transport processes revisited. *International Journal of Heat and Mass Transfer, 189*, 122699. [CrossRef]

[40] Malvandi, A., Ganji, D. D., Hedayati, F., & Rad, E. Y. (2013). An analytical study on entropy generation of nanofluids over a flat plate. *Alexandria Engineering Journal, 52*(4), 595-604. [CrossRef]

[41] Afridi, M. I., Qasim, M., & Shafie, S. (2017). Entropy generation in hydromagnetic boundary flow under the effects of frictional and Joule heating: Exact solutions. *The European Physical Journal Plus, 132*(9), 404. [CrossRef]

[42] Khan, M., Azam, M., & Alshomrani, A. S. (2017). Effects of melting and heat generation/absorption on unsteady Falkner-Skan flow of Carreau nanofluid over a wedge. *International Journal of Heat and Mass Transfer, 110*, 437–446. [CrossRef]

[43] Hayat, T., Shafique, M., Tanveer, A., & Alsaedi, A. (2017). Slip and Joule heating effects on radiative peristaltic flow of hyperbolic tangent nanofluid. *International Journal of Heat and Mass Transfer, 112*, 559–567. [CrossRef]

[44] Rehman, S., Hashim, Alqahtani, S., Ben Hadj Hassine, S., & Eldin, S. M. (2023). Thermohydraulic and irreversibility assessment of Power-law fluid flow within wedge shape channel. *Arabian Journal of Chemistry, 16*(3), 104475. [CrossRef]

[45] Rosseland, S. (1931). *Astrophysik: Auf atomtheoretischer Grundlage*. Springer. [CrossRef]

[46] Hashim, Rehman, S., Alqahtani, S., Alshehery, S., & Ben Moussa, S. (2023). A comprehensive physical insight of inclined magnetic field on the flow of generalized Newtonian fluid within a conduit with homogeneous-heterogeneous reactions. *Arabian Journal of Chemistry, 16*(5), 104633. [CrossRef]

[47] Nayak, M. K., Mabood, F., Dogonchi, A. S., & Khan, W. A. (2021). Electromagnetic flow of SWCNT/MWCNT suspensions with optimized entropy generation and cubic auto catalysis chemical reaction. *International Communications in Heat and Mass Transfer, 120*, 104996. [CrossRef]

[48] Khan, M. I., Khan, S. A., Hayat, T., Khan, M. I., & Alsaedi, A. (2019). Nanomaterial based flow of Prandtl-Eyring (non-Newtonian) fluid using Brownian and thermophoretic diffusion with entropy generation. *Computer Methods and Programs in Biomedicine, 180*, 105017. [CrossRef]

[49] Vajravelu, K., & Mukhopadhyay, S. (2015). *Fluid flow, heat and mass transfer at bodies of different shapes: numerical solutions*. Academic Press. [CrossRef]

[50] Mukhopadhyay, S. (2012). Effects of radiation and variable fluid viscosity on flow and heat transfer along a symmetric wedge. *Journal of Applied Fluid Mechanics, 2*(2), 29–34. [CrossRef]

[51] Mukhopadhyay, S., & Bhattacharyya, K. (2014). Boundary layer flow and heat transfer of a Casson fluid past a symmetric porous wedge with surface heat flux. *Chinese Physics B, 23*(4), 044702. [CrossRef]

[52] Watanabe, T. (1990). Thermal boundary layers over a wedge with uniform suction or injection in forced flow. *Acta Mechanica, 83*(3), 119–126. [CrossRef]

[53] Yacob, N. A., Ishak, A., & Pop, I. (2011). Falkner–Skan problem for a static or moving wedge in nanofluids. *International Journal of Thermal Sciences, 50*(2), 133–139. [CrossRef]

[54] Berrehal, H., Maougal, A., Hayat, T., & Alsaedi, A. (2018, December). On the analytic solution of magnetohydrodynamic (MHD) flow by a moving wedge in porous medium. In *Defect and Diffusion Forum* (Vol. 389, pp. 128-137). Trans Tech Publications Ltd. [CrossRef]

[55] Berrehal, H., & Maougal, A. (2019). Entropy generation analysis for multi-walled carbon nanotube (MWCNT) suspended nanofluid flow over wedge with thermal radiation and convective boundary condition. *Journal of Mechanical Science and Technology, 33*(1), 459-464. [CrossRef]

[56] Kuo, B. L. (2005). Heat transfer analysis for the Falkner–Skan wedge flow by the differential transformation method. *International Journal of Heat and Mass Transfer, 48*(23-24), 5036-5046. [CrossRef]

[57] Butt, A. S., Munawar, S., Ali, A., & Mehmood, A. (2012). Entropy generation in the Blasius flow under thermal radiation. *Physica Scripta, 85*(3), 035008. [CrossRef]

[58] Mansur, S., & Ishak, A. (2016). Unsteady boundary layer flow of a nanofluid over a stretching/shrinking sheet with a convective boundary condition. *Journal of the Egyptian Mathematical Society, 24*(4), 650-655. [CrossRef]

[59] Grötzbach, G. (2013). Challenges in low-Prandtl number heat transfer simulation and modelling. *Nuclear engineering and design, 264*, 41-55. [CrossRef]

Sohail Rehman received the Ph.D. degree in Applied Mathematics from Islamia College Peshawar, Pakistan. He is currently working as an Assistant Professor in the Department of Physical and Numerical Sciences at Qurtuba University Peshawar, Pakistan. His broader research interests include the study of non-Newtonian fluid flows, heat and mass transfer problems, nanofluids, magnetohydrodynamics (MHD), entropy generation analysis, and computational fluid dynamics. He has published extensively in well-renowned international journals, including *Applied Mathematics and Computation*, *International Communications in Heat and Mass Transfer*, *Case Studies in Thermal Engineering*, *Ain Shams Engineering Journal*, *Journal of the Taiwan Institute of Chemical Engineers*, *Alexandria Engineering Journal*, *Advances in Engineering Software*, *Nanotechnology Reviews*, and *Nonlinear Engineering*, among others. (Email: sohail08ktk@gmail.com)